Dispersion of elastic waves in a strongly inhomogeneous three-layered plate

J. Kaplunov*, D.A. Prikazchikov, L.A. Prikazchikova

School of Computing and Mathematics, Keele University
Keele, Staffordshire, ST5 5BG, UK

Abstract

Elastic wave propagation in a three-layered plate with high-contrast mechanical and geometric properties of the layers is analysed. Four specific types of contrast arising in engineering practice, including the design of stiff and lightweight structures, laminated glass, photovoltaic panels, and electrostatic precipitators in gas filters, are considered. For all of them the cut-off frequency of the first harmonic is close to zero. Two-mode asymptotic polynomial expansions of the Rayleigh-Lamb dispersion relation approximating both the fundamental bending wave and the first harmonic, are derived. It is established that these can be either uniform or composite ones, valid only over non-overlapping vicinities of zero and the lowest cut-off frequencies. The partial differential equations of motion associated with two-mode shortened dispersion relations are also presented.

Keywords: Vibration, sandwich plate, asymptotic, contrast.

1. Introduction

Multi-layered engineering structures, in particular three-layered symmetric plates and shells, also known as sandwich structures, have been manufactured since long ago. Sandwich structures, due to their light weight combined with relatively large flexural stiffness, are in a great demand for modern aerospace, automotive, and civil engineering, e.g. see Vinson (1999) and references therein.

Recent technological developments intensively exploit structures with high contrast in material and geometrical properties of the layers, including, for example, laminated glass beams and plates widely used in glazing and photovoltaic applications. Laminated glass is usually designed as a three-layered plate, with two stiff

*Corresponding author
Email addresses: j.kaplunov@keele.ac.uk (J. Kaplunov), d.prikazchikov@keele.ac.uk (D.A. Prikazchikov), l.prikazchikova@keele.ac.uk (L.A. Prikazchikova)

facings and a soft polymeric interlayer, see Schulze et al. (2012) and Aşık & Tezcan (2005). For photovoltaic panels, the ratio of the shear moduli of a glass skin and polymeric layer encapsulating solar cells, is within the range $10^{-5} \sim 10^{-2}$, depending on temperature and polymer type, see Schulze et al. (2012), Altenbach et al. (2015), Aßmus et al. (2016), Aßmus et al. (2017), and Naumenko & Eremeyev (2014). In automotive and civil engineering, laminated glass has a rather thin polymeric core layer with relatively thick glass facings, resulting in a substantial contrast of core and skin layer thicknesses. Another advanced application of multi-layered structures with high-contrast material properties is connected with the rapidly growing area of meta-materials, e.g. see Martin et al. (2012).

All of the aforementioned structures are characterised by stiff facings. However, there are also important examples of structures with soft facings and a stiff core layer. In particular, this is a feature of dust-covered precipitator plates, which are important parts of gas filters reducing air pollution Lee & Chang (1979).

Mechanics of layered media, including sandwich structures, without a special emphasis on high contrast problems, has been thoroughly investigated, e.g. see the textbooks Qatu (2004), Wang et al. (2000), Reddy (2004), and Milton (2002) to name a few. Numerous publications deal with sandwich plates and beams, e.g. see review articles Hohe & Librescu (2004), Kreja (2011), and Carrera & Brischetto (2009).

At the same time only a few considerations are oriented towards strongly inhomogeneous multi-layered structures. Among them, we mention asymptotic developments on the subject reported in Berdichevsky (2010), Kudaibergenov et al. (2016), Tovstik & Tovstik (2016), and Kaplunov et al. (2016), along with Altenbach et al. (2015) and Naumenko & Eremeyev (2014) using ad hoc layerwise theories, and Chapman (2013) developing finite-product approximations to the exact Rayleigh-Lamb dispersion relation for a three-layered plate. In addition, we cite Cherdantsev & Cherednichenko (2012), Smyshlyaev (2009), Figotin & Kuchment (1998), and Kaplunov & Nobili (2016) devoted to homogenization of high-contrast periodic composites. Similarity of the asymptotic procedures underlying multi-layered plate theories and homogenization for periodic media has been recently reported in Craster et al. (2014).

In this paper we present results of the asymptotic analysis of the exact dispersion relation corresponding to plane anti-symmetric waves propagating in a three-layered elastic plate. The main focus is on the set of problem parameters, for which the lowest thickness shear resonance frequency tends to zero at a high-contrast limit, see Kaplunov et al. (2016) dealing with the identical 1D problem for an elastic

rod, and also Lee & Chang (1979) and Ryazantseva & Antonov (2012) studying a sandwich plate. This cut-off frequency seemingly determines the upper bound of the frequency domain, in which the asymptotic formulation in Berdichevsky (2010) initially oriented to statics, is applicable.

Four specific setups are studied, including stiff skin layers and light core layer, stiff thin skin layers and light core layer, stiff skin layers and thin light core layer, soft thin skin layers and light core layer. Shortened polynomial dispersion relations, governing long-wave low-frequency behaviour, e.g. see Kaplunov et al. (1998), are derived. All of them approximate both the fundamental and the lowest shear vibration modes. It is remarkable that the obtained asymptotic expansions are uniformly valid only for plates with stiff skin layers and light core layer, and stiff skin layers and thin light core layer. Other setups allow only the so-called 'composite' expansions, e.g. see Van Dyke (1975) and Andrianov et al. (2013), valid only over non-overlapping vicinities of zero and the lowest thickness resonance frequencies.

The accuracy of the established two-mode approximations is tested by numerical comparisons with the solutions of the Rayleigh-Lamb dispersion relation. The ranges of applicability of the local one-mode approximations valid near zero and the lowest shear thickness resonance frequencies, are also evaluated. In addition, we present numerical data for cross-thickness variations of plate displacements.

Finally, we restore partial differential equations of motion starting from the established two-mode dispersion relations. This finding is preceded by preliminary remarks emphasising an important correspondence between shortened polynomial dispersion relations and long-wave plate theories.

2. Preliminary remarks

Consider first an isotropic layer of thickness $2h$ and infinite lateral extent. Without loss of generality restrict ourselves to plane antisymmetric motion. In this case the Rayleigh-Lamb dispersion relation for a layer with traction-free faces takes the form, e.g. see Graff (2012),

$$\gamma^4 \frac{\sinh\alpha}{\alpha}\cosh\beta - \beta^2 K^2 \cosh\alpha \frac{\sinh\beta}{\beta} = 0, \tag{1}$$

with

$$\alpha^2 = K^2 - \varkappa^2\Omega^2, \quad \beta^2 = K^2 - \Omega^2, \quad \gamma^2 = K^2 - \frac{1}{2}\Omega^2. \tag{2}$$

In the above

$$K = kh, \quad \Omega = \frac{\omega h}{c_2}, \quad \varkappa = \frac{c_2}{c_1}. \tag{3}$$

Here ω is the angular frequency, k is the wave number, c_1 and c_2 are the longitudinal and shear wave speeds, respectively, given by

$$c_1^2 = \frac{\lambda + 2\mu}{\rho}, \qquad c_2^2 = \frac{\mu}{\rho}, \tag{4}$$

where λ and μ are the Lamé constants, and ρ is volume mass density.

The transcendental dispersion relation (1) allows polynomial asymptotic expansions at the long wave limit $K \ll 1$; here and below in this section see Kaplunov et al. (1998) for further detail. Over the low frequency domain $\Omega \ll 1$, we have for the fundamental vibration mode at leading order

$$K^4 \approx D_0^{-1}\Omega^2, \tag{5}$$

with

$$D_0 = \frac{2}{3(1-\nu)}$$

indicating that $\Omega \sim K^2$. This shortened dispersion relation also follows from the classical Kirchhoff theory of plate bending, governed by the 1D equation

$$D_0 \frac{d^4 w}{d\xi^4} - \Omega^2 w = 0, \tag{6}$$

where w is the vertical displacement and ξ is the longitudinal coordinate normalised by the plate half-thickness h.

Over the high-frequency domain $\Omega \sim 1$, long-wave asymptotic expansions can only be derived near the thickness resonances that determine the cut-off frequencies for harmonics. The lowest cut-off frequency correponds to the first shear thickness resonance and is given by $\Omega = \pi/2$. Over the vicinity of $\Omega - \pi/2$ we get for the first harmonic at leading order

$$K^2 \approx P^{-1}\left(\Omega^2 - \frac{\pi^2}{4}\right), \tag{7}$$

where

$$P = 1 + \frac{16}{\pi}\varkappa \cot\left(\frac{\varkappa\pi}{2}\right).$$

This corresponds to the following 1D equation

$$P\frac{d^2 w}{d\xi^2} + \left(\Omega^2 - \frac{\pi^2}{4}\right) w = 0. \tag{8}$$

It is obvious that the ranges of validity of the low- and high-frequency asymptotic expansions (5) and (7), as well as those of the associated differential equations (6) and (8), do not overlap. In fact, (5) and (6) are valid only at $\Omega \ll 1$, whereas (7) and (8) are applicable at $\Omega - \pi/2 \ll 1$, i.e. at $\Omega \sim 1$. This is why a two-mode uniform

long wave asymptotic expansion and consequently uniformly valid plate theory, approximating the fundamental mode and the first harmonic simultaneously, can not be constructed.

However, there is still a possibility of composite formulations, see e.g. Van Dyke (1975) and Andrianov et al. (2013), asymptotically justified only at the local high-frequency and low-frequency long-wave limits, but not over the whole frequency range. For example, composite structural models, see Berdichevsky (2009) and Le (1999), may bring a sort of mathematical validation for ad hoc Timoshenko-Reissner-Mindlin type theories, see e.g. Elishakoff et al. (2015) and references therein, popular among the engineering community. The limits of applicability of Timoshenko-Reissner model for multi-layered plates and beams in case of contrasting Young moduli of the layers are addressed in Tovstik & Tovstik (2016).

A composite equation originating from (6) and (8) may be written as

$$\overbrace{D_0\frac{d^4w}{d\xi^4}-\Omega^2 w}^{\text{low-frequency}}+\underbrace{\frac{4}{\pi^2}\Omega^2\left(P\frac{d^2w}{d\xi^2}+\Omega^2 w\right)}_{\text{high-frequency}}=0.$$

The related dispersion relation is

$$D_0K^4-\Omega^2+\frac{4}{\pi^2}\Omega^2\left(\Omega^2-K^2P\right)=0. \tag{9}$$

It can be easily verified that at the long-wave limits ($K \ll 1$ and $\Omega \ll 1$ or $\Omega-\pi/2 \ll 1$) this relation reduces to (5) and (7), respectively. At the same time it can not be asymptotically justified for the intermediate frequencies $\Omega \sim 1$. The associated gap within the range of validity of the composite dispersion relation (9) is clearly seen in Figure 1. In this figure the dispersion curves (1) and their composite approximation (9) are plotted for $\varkappa = 0.53$, corresponding to the Poisson ratio $\nu = 0.3$.

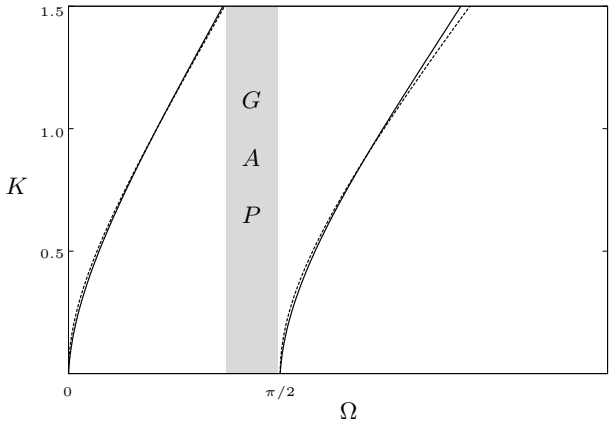

Figure 1: Dispersion curves for the composite approximation (9) (dashed line) and the Rayleigh-Lamb dispersion relation (1) (solid line) at $\nu = 0.3$

In what follows, we show that, in contrast to the consideration above, the Rayleigh-Lamb dispersion relation for a three-layered strongly inhomogeneous plate allows two-mode uniform asymptotic expansions for several sets of problem parameters.

3. Statement of the problem

Consider 2D harmonic vibrations of a mid-plane symmetric three-layered elastic plate with core and skin layers of thickness h_c and h_s, respectively, see Figure 2.

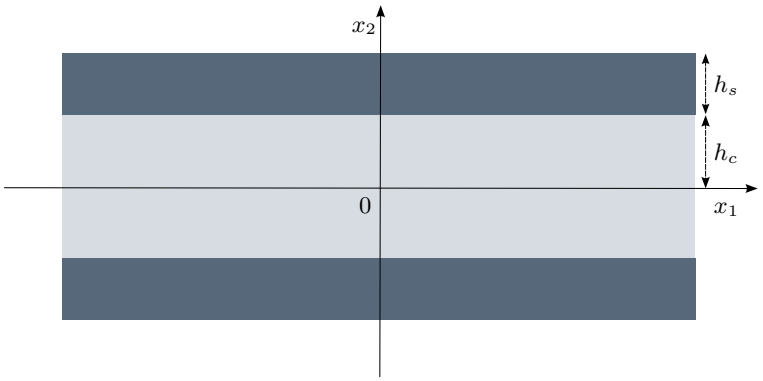

Figure 2: A three-layered plate

The equations of motion for core and skin layers are taken in the form

$$\sigma^q_{ij,j} = \rho_q \ddot{u}^q_i, \quad i = 1, 2, \quad q = c, s \tag{10}$$

with the index q taking the values $q = c$ and $q = s$ for the core and skin layers,
105 respectively; summation over the repeated suffixes is assumed. Here σ_{ij}^q are stresses, u_i are displacements, ρ_q are volume mass densities.

The constitutive relations for a linearly isotropic material are given by

$$\sigma_{ij}^q = \lambda_q \varepsilon_{kk}^q \delta_{ij} + 2\mu_q \varepsilon_{ij}^q, \tag{11}$$

with

$$\varepsilon_{ij}^q = \frac{1}{2}(u_{i,j}^q + u_{j,i}^q), \quad q = c, s, \tag{12}$$

where ε_{ij}^q are strains, and λ_q and μ_q are the Lamé parameters.

The traction free boundary conditions

$$\sigma_{12}^s = \sigma_{22}^s = 0 \tag{13}$$

along the faces $x_2 = \pm(h_c + h_s)$ are imposed, together with the continuity conditions

$$\sigma_{12}^c = \sigma_{12}^s, \quad \sigma_{22}^c = \sigma_{22}^s, \quad u_1^c = u_1^s, \quad u_2^c = u_2^s \tag{14}$$

along the interfaces $x_2 = \pm h_c$.

Let us define the dimensionless frequency Ω and wave number K as

$$\Omega = \frac{\omega h_c}{c_{2c}}, \qquad K = k h_c, \tag{15}$$

and introduce the dimensionless parameters

$$h = \frac{h_s}{h_c}, \qquad \varepsilon = \frac{\mu_c}{\mu_s}, \qquad r = \frac{\rho_c}{\rho_s}, \tag{16}$$

expressing the contrast in thickness, stiffness and density of the core and skin layers.

The dispersion relation for the antisymmetric modes of the plate governed by the equations above, can be written as, e.g. see Lee & Chang (1979),

$$\begin{aligned}
&4K^2h^3\alpha_s\beta_s F_4\left[F_1F_2C_{\beta_c}S_{\alpha_c} - 2\alpha_c\beta_c(\varepsilon-1)F_3C_{\alpha_c}S_{\beta_c}\right] + \\
&h\alpha_s\beta_s C_{\alpha_s}C_{\beta_s}\left[4\alpha_c\beta_c K^2\left(h^4F_3^2 + {F_4}^2(\varepsilon-1)^2\right)C_{\alpha_c}S_{\beta_c} - \right. \\
&\qquad\qquad \left.\left(4K^4h^4F_2^2 + {F_4}^2F_1^2\right)S_{\alpha_c}C_{\beta_c}\right] + \\
&C_{\beta_s}S_{\alpha_s}\varepsilon\beta_s(\beta_s^2 - K^2h^2)(\beta_c^2 - K^2)\left[4\alpha_s^2\beta_c K^2h^2S_{\alpha_c}S_{\beta_c} - {F_4}^2\alpha_c C_{\alpha_c}C_{\beta_c}\right] + \\
&C_{\alpha_s}S_{\beta_s}\varepsilon\alpha_s(\beta_s^2 - K^2h^2)(\beta_c^2 - K^2)\left[4\alpha_c\beta_s^2K^2h^2C_{\alpha_c}C_{\beta_c} - {F_4}^2\beta_c S_{\alpha_c}S_{\beta_c}\right] + \\
&h^3S_{\alpha_s}S_{\beta_s}\left[\left(4\alpha_s^2\beta_s^2K^2F_1^2 + K^2{F_4}^2F_2^2\right)C_{\beta_c}S_{\alpha_c} - \right. \\
&\qquad\qquad \left.\alpha_c\beta_c\left(16\alpha_s^2\beta_s^2(\varepsilon-1)^2K^4 + {F_4}^2F_3^2\right)C_{\alpha_c}S_{\beta_c}\right] = 0,
\end{aligned} \tag{17}$$

where

$$
\begin{aligned}
F_1 &= 2(\varepsilon-1)K^2 - \varepsilon\Omega^2,\\
F_2 &= 2(\varepsilon-1)K^2 + \frac{\varepsilon(1-r)}{r}\,\Omega^2,\\
F_3 &= 2(\varepsilon-1)K^2 + \frac{\varepsilon}{r}\,\Omega^2,\\
F_4 &= \beta_s^2 + K^2h^2,
\end{aligned}
\tag{18}
$$

and

$$
\begin{aligned}
&\alpha_c^2 = K^2 - \varkappa_c^2\Omega^2, \quad \alpha_s^2 = h^2\left(K^2 - \frac{\varepsilon\varkappa_s^2}{r}\,\Omega^2\right),\\
&\beta_c^2 = K^2 - \Omega^2, \quad \beta_s = h^2\left(K^2 - \frac{\varepsilon}{r}\,\Omega^2\right).
\end{aligned}
\tag{19}
$$

In the above $C_{\alpha_q} = \cosh(\alpha_q)$, $C_{\beta_q} = \cosh(\beta_q)$, $S_{\alpha_q} = \sinh(\alpha_q)$, $S_{\beta_q} = \sinh(\beta_q)$, and $\varkappa_q = c_{2q}/c_{1q}$ with

$$
c_{1q}^2 = \frac{\lambda_q + 2\mu_q}{\rho_q}, \quad c_{2q}^2 = \frac{\mu_q}{\rho_q}, \quad q = c, s. \tag{20}
$$

On introducing the dimensionless variable $\chi = x_2/h_c$ the displacements of the core ($|\chi| \le 1$) and skins ($1 \le |\chi| \le 1+h$) are given by

$$
\begin{aligned}
u_{1c} &= iKA_c\sinh(\alpha_c\chi) - \beta_cB_c\sinh(\beta_c\chi),\\
u_{2c} &= \alpha_cA_c\cosh(\alpha_c\chi) + iKB_c\cosh(\beta_c\chi),
\end{aligned}
\tag{21}
$$

and

$$
\begin{aligned}
u_{1s} &= iK[A_s\sinh(\theta_s\chi) + B_s\cosh(\theta_s\chi)] - \kappa_s[D\cosh(\kappa_s\chi) + \sinh(\kappa_s\chi)],\\
u_{2s} &= \theta_s[A_s\cosh(\theta_s\chi) + B_s\sinh(\theta_s\chi)] + iK[D\sinh(\kappa_s\chi) + \cosh(\kappa_s\chi)],
\end{aligned}
\tag{22}
$$

with $\theta_s = \alpha_s/h$, $\kappa_s = \beta_s/h$ and the constants A_c, A_s, B_c, B_s, and D presented in Appendix A.

The dispersion curves for two sets of problem parameters are demonstrated in Figure 3 ($\varepsilon = 0.232$, $h = 1.0$, $r = 3.0$, $\varkappa_c \approx 0.58$, and $\varkappa_s \approx 0.30$) and in Figure 4 ($\varepsilon = 0.014$, $h = 1.0$, $r = 0.03$, $\varkappa_c \approx 0.53$, and $\varkappa_s \approx 0.46$). Numerical data in Figure 3 is similar to that for a homogeneous plate, see Figure 1, whereas the lowest shear thickness resonance $\Omega = 0.17$ being the cut-off of the first harmonic in Figure 4 is close to zero. This is due to a high contrast in density and stiffness of the core and skin layers, resulting in the small parameters r and ε defined by (16).

The consideration below is centered around a high-contrast plate, for which the value of the lowest thickness shear resonance is asymptotically small. In this case we may expect that not only the fundamental vibration mode, but also the first harmonic appear in the low frequency domain. This is not a feature of a homogeneous plate, for which the first harmonic arises only at $\Omega \sim 1$, see (7).

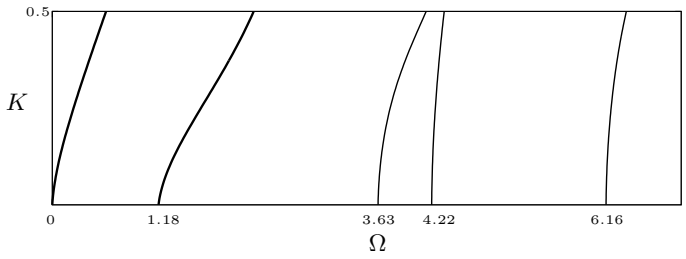

Figure 3: Dispersion curves for a three-layered plate with no contrast at $\varepsilon = 0.232$, $h = 1.0$, $r = 3.0$, $\varkappa_c \approx 0.58$, and $\varkappa_s \approx 0.30$.

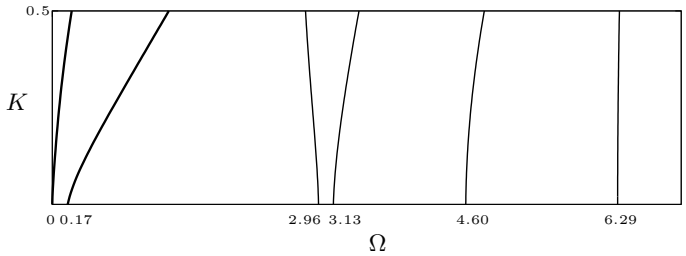

Figure 4: Dispersion curves for a strongly inhomogeneous three-layered plate with high contrast properties at $\varepsilon = 0.014$, $h = 1.0$, $r = 0.03$, $\varkappa_c \approx 0.53$, and $\varkappa_s \approx 0.46$.

4. Asymptotic approach

First, derive the conditions on material and geometrical parameters ensuring the lowest shear resonant frequency to be small. To this end, study a 1D eigenvalue problem along the plate cross section, see Kaplunov et al. (1998) for more detail. On setting in the equations in the previous sections $\partial u_1^q/\partial x_1 = u_2^q = 0$, $q = c, s$, we have

$$\frac{\partial^2 u_1^q}{\partial x_2^2} + \frac{\omega^2}{c_2^q} u_1^q = 0, \qquad q = c, s, \tag{23}$$

together with the boundary and continuity conditions

$$\frac{\partial u_1^s}{\partial x_2} = 0 \quad \text{at} \quad x_2 = \pm(h_c + h_s),$$
$$\mu_c \frac{\partial u_1^c}{\partial x_2} = \mu_s \frac{\partial u_1^s}{\partial x_2}, \quad u_1^c = u_2^s \quad \text{at} \quad x_2 = \pm h_c.$$

Similarly to Kaplunov et al. (2016), see also Ryazantseva & Antonov (2012), we arrive at the frequency equation

$$\tan(\Omega) \tan\left(\left(\frac{\varepsilon}{r}\right)^{1/2} h\,\Omega\right) = (\varepsilon r)^{1/2}, \tag{24}$$

inferring that for the contrast parameters satisfying

$$r \ll h \ll \varepsilon^{-1}, \tag{25}$$

the lowest eigenvalue is small, given at leading order by

$$\Omega_{sh} \approx \left(\frac{r}{h}\right)^{1/2} \ll 1. \tag{26}$$

At leading order the associated eigensolution has the following piecewise linear variation across the thickness, see Figure 5,

$$u_1^{sh} = \begin{cases} \chi, & \text{for } |\chi| \le 1 \\ 1, & \text{for } 1 \le |\chi| \le 1+h, \end{cases} \tag{27}$$

with $\chi = x_2/h_c$, which is typical for the so-called global low-frequency behaviour defined in Kaplunov et al. (2016). It is worth noting that under the conditions (25) the eigenmode (27) is the only one demonstrating piecewise linear variation across the plate thickness.

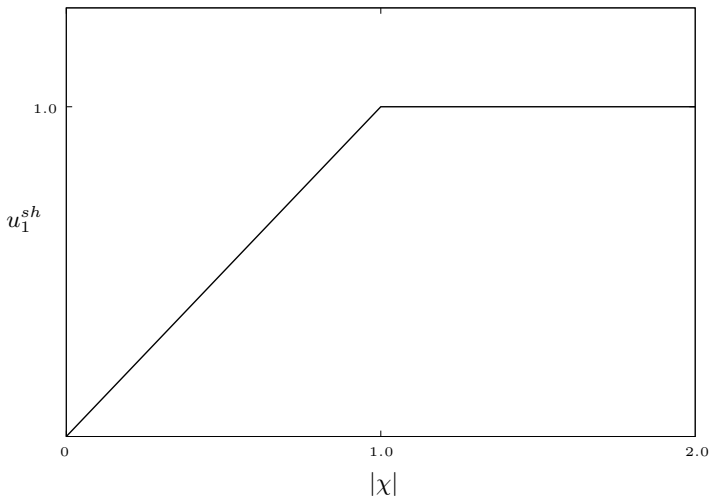

Figure 5: The lowest shear eigenmode (27)

Let us derive the long-wave low-frequency asymptotic expansions of the transcendental Rayleigh-Lamb equation (17) over the parameter range (25) assuming that

$$K(1+h) \ll 1, \qquad \Omega\left(1 + h\left(\frac{\varepsilon}{r}\right)^{1/2}\right) \ll 1. \tag{28}$$

In this case the hyperbolic functions in (17) may be expanded into asymptotic series, finally resulting in the polynomial dispersion relation

$$\begin{aligned} &\gamma_1\Omega^2 + \gamma_2 K^4 + \gamma_3 K^2\Omega^2 + \gamma_4 K^6 + \gamma_5\Omega^4 + \gamma_6 K^4\Omega^2 + \gamma_7 K^8 + \\ &\gamma_8 K^2\Omega^4 + \gamma_9 K^6\Omega^2 + \gamma_{10} K^{10} + ... = 0, \end{aligned} \tag{29}$$

where the coefficients γ_i are given explicitly in Appendix B.

Next, we express the contrast parameters r and h in (16) through ε as

$$h \sim \varepsilon^a, \quad r \sim \varepsilon^b, \tag{30}$$

not making any preliminary assumptions regarding the asymptotic order of ε and the sign of the constants a and b. Consequently, we estimate the coefficients γ_i in (29) as $\gamma_i \to G_i\varepsilon^c$, where $G_i \sim 1$ and c is a constant.

Below we study two-mode shortened forms of the dispersion relation for the four different types of contrast satisfying the strong inequalities (25), see Figure 6. Analysis of the three-layered structures in this figure is inspired by various engineering applications, including photovoltaic panels (Figure 6a), sandwich constructions (Figure 6b), laminated glass(Figure 6c), plate precipitators in gas filters (Figure 6d), e.g. see Vinson (1999), Schulze et al. (2012), Naumenko & Eremeyev (2014), and Lee & Chang (1979).

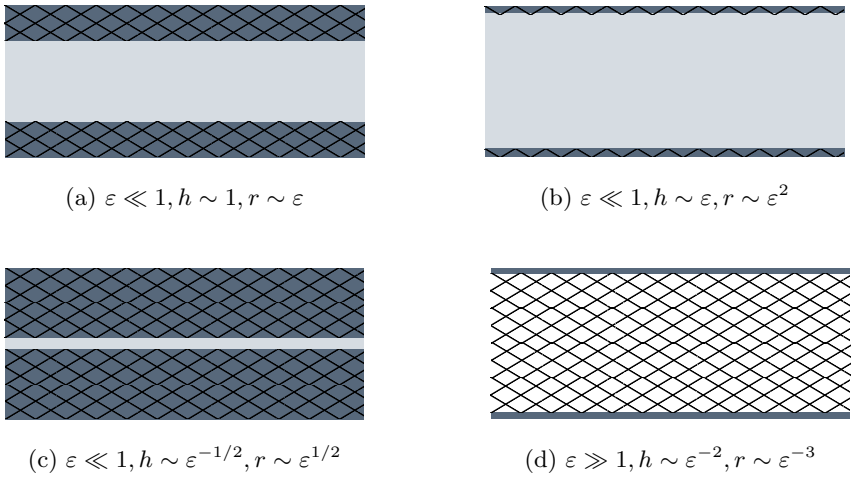

(a) $\varepsilon \ll 1, h \sim 1, r \sim \varepsilon$ (b) $\varepsilon \ll 1, h \sim \varepsilon, r \sim \varepsilon^2$

(c) $\varepsilon \ll 1, h \sim \varepsilon^{-1/2}, r \sim \varepsilon^{1/2}$ (d) $\varepsilon \gg 1, h \sim \varepsilon^{-2}, r \sim \varepsilon^{-3}$

Figure 6: Types of contrast: a) stiff skin layers and light core layer, b) stiff thin skin layers and light core layer, c) stiff skin layers and thin light core layer, d) soft thin skin layers and light core layer.

5. Stiff skin layers and light core layer ($\varepsilon \ll 1$, $h \sim 1$, and $r \sim \varepsilon$)

The asymptotic results are summarised in Table 1. In particular, the limiting behaviour of the coefficients γ_i in the polynomial equation (29) as $\varepsilon \ll 1$ are listed in the first column of Table 1.

Order of γ_i	Terms	Fundamental mode $K \sim \Omega^{1/2}$ $\Omega \ll 1$	Harmonic $K \sim \left(\Omega^2 - \Omega_{sh}^2\right)^{1/2}$ $\Omega_{sh} \le \Omega \ll 1$
$\gamma_1 \sim \varepsilon$	$\gamma_1 \Omega^2$	εK^4	$\varepsilon(\varepsilon + K^2)$
$\gamma_2 \sim \varepsilon$	$\gamma_2 K^4$	εK^4	εK^4
$\gamma_3 \sim 1$	$\gamma_3 K^2 \Omega^2$	K^6	$K^2(\varepsilon + K^2)$
$\gamma_4 \sim 1$	$\gamma_4 K^6$	K^6	K^6
$\gamma_5 \sim 1$	$\gamma_5 \Omega^4$	K^8	$(\varepsilon + K^2)^2$
$\gamma_6 \sim 1$	$\gamma_6 K^4 \Omega^2$	K^8	$K^4(\varepsilon + K^2)$
$\gamma_7 \sim 1$	$\gamma_7 K^8$	K^8	K^8
$\gamma_8 \sim 1$	$\gamma_8 \Omega^4 K^2$	K^{10}	$K^2(\varepsilon + K^2)^2$
$\gamma_9 \sim 1$	$\gamma_9 K^6 \Omega^2$	K^{10}	$K^6(\varepsilon + K^2)$
$\gamma_{10} \sim 1$	$\gamma_{10} K^{10}$	K^{10}	K^{10}

Table 1: Asymptotic behaviour at $\varepsilon \ll 1$, $h \sim 1$, and $r \sim \varepsilon$

The expressions through the wave number are displayed in the third column for the fundamental mode and in the fourth column for the first harmonic, for which the cut-off frequency is $\Omega_{sh} \sim \varepsilon^{1/2}$ according to (26), see (28).

Let us neglect all of the asymptotically secondary terms at $K \ll 1$ in the second column of Table 1, using the data from the first, third, and fourth columns. Then, we get

$$\varepsilon G_1 \Omega^2 + \varepsilon G_2 K^4 + G_3 K^2 \Omega^2 + G_4 K^6 + G_5 \Omega^4 = 0, \tag{31}$$

where at leading order

$$\begin{aligned} &G_1 = -\frac{h^6}{r_0^3}, \quad G_2 = -\frac{4}{3}\frac{h^6(\varkappa_s^2 - 1)(h^2 + 3h + 3)}{r_0^2}, \quad G_3 = \frac{4h^7(\varkappa_s^2 - 1)}{r_0^3}, \\ &G_4 = \frac{4}{3}\frac{h^9(\varkappa_s^2 - 1)^2}{r_0^2}, \quad G_5 = \frac{h^7}{r_0^4}, \end{aligned} \tag{32}$$

with $r_0 = r/\varepsilon$.

This is a uniform two-mode expansion of the Rayleigh-Lamb dispersion equation, valid over the entire low-frequency range $\Omega \ll 1$ in (28) for both the fundamental mode and the first harmonic, see the numerical illustration in Figure 7 for $\varepsilon = 0.014$, $h = 1.0$, $r = 0.03$, $\varkappa_c \approx 0.53$, and $\varkappa_s \approx 0.46$.

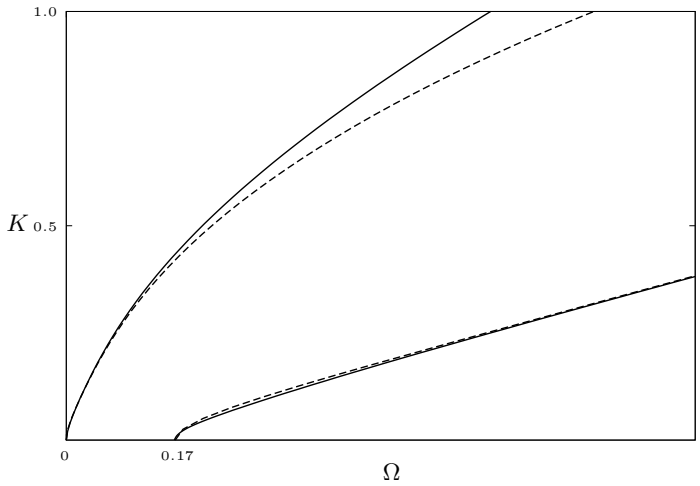

Figure 7: Dispersion curves for two-mode approximation (31) (dashed line) and the Rayleigh-Lamb dispersion relation (17) (solid line) at $\varepsilon = 0.014$, $h = 1.0$, $r = 0.03$, $\varkappa_c \approx 0.53$, and $\varkappa_s \approx 0.46$.

The related uniform approximation for the fundamental mode takes the form, see Table 1,

$$\varepsilon G_1 \Omega^2 + \varepsilon G_2 K^4 + G_3 K^2 \Omega^2 + G_4 K^6 = 0. \tag{33}$$

The local approximations of the latter are given by

$$G_1 \Omega^2 + G_2 K^4 = 0, \quad \Omega \ll \varepsilon, \tag{34}$$

and

$$G_3 \Omega^2 + G_4 K^4 = 0, \quad \varepsilon \ll \Omega \ll 1. \tag{35}$$

It is worth mentioning that in the transition region $\Omega = \delta\varepsilon$ ($\delta \sim 1$) the uniform expansion (33) becomes

$$\varepsilon^3 \delta^2 G_1 + \varepsilon G_2 K^4 + \varepsilon^2 \delta^2 G_3 K^2 + G_4 K^6 = 0 \tag{36}$$

implying that $K \sim \varepsilon^{1/2}$ for both local approximations for the fundamental mode as in the classical theory for plate bending Kaplunov et al. (1998).

Numerical data validating the shortened dispersion relations (33), (34), and (35) are given in Figures 8 and 9 for the same set of problem parameters as in Figure 7. As before, the Rayleigh-Lamb dispersion relation is chosen as a benchmark.

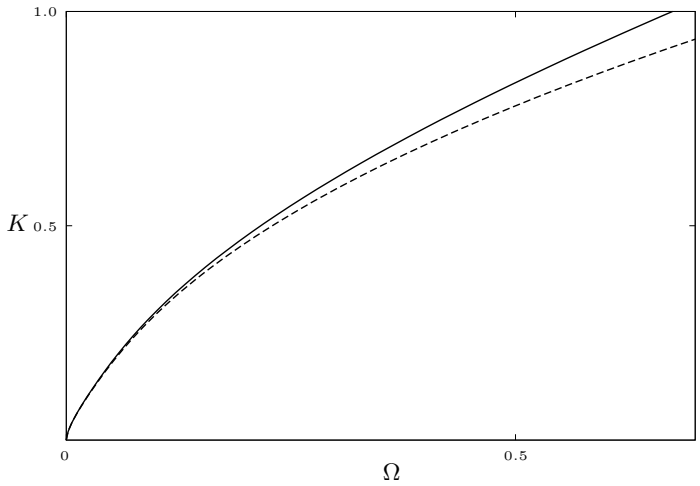

Figure 8: Dispersion curves for the uniform asymptotic expansion (33) (dashed line) and the Rayleigh-Lamb dispersion relation (17) (solid line)

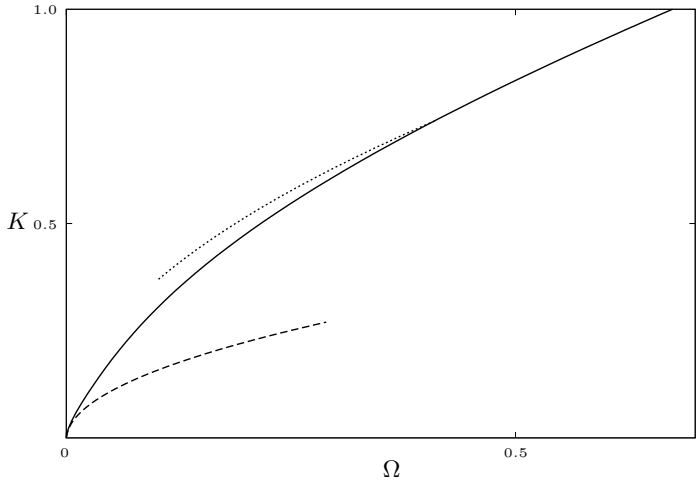

Figure 9: Dispersion curves for the two local approximations (34)(dashed line) and (35) (dotted line) and the Rayleigh-Lamb dispersion relation (17) (solid line)

The asymptotic expansion for the first harmonic takes the form

$$\varepsilon G_1 + G_3 K^2 + G_5 \Omega^2 = 0, \quad \Omega_{sh} \leq \Omega \ll 1. \tag{37}$$

Therefore, as usual for a near cut-off expansion, e.g. see Kaplunov et al. (1998),

$$\Omega^2 = \Omega_{sh}^2 + 4r_0(1 - \varkappa_s^2)K^2 + ..., \tag{38}$$

where

$$\Omega_{sh}^2 = \varepsilon \frac{r_0}{h}. \tag{39}$$

A numerical illustration of (37) is displayed in Figure 10.

Outside a narrow vicinity of the cut-off, the equation (37) can be simplified to

$$G_3K^2 + G_5\Omega^2 = 0, \quad \Omega_{sh} \ll \Omega \ll 1. \tag{40}$$

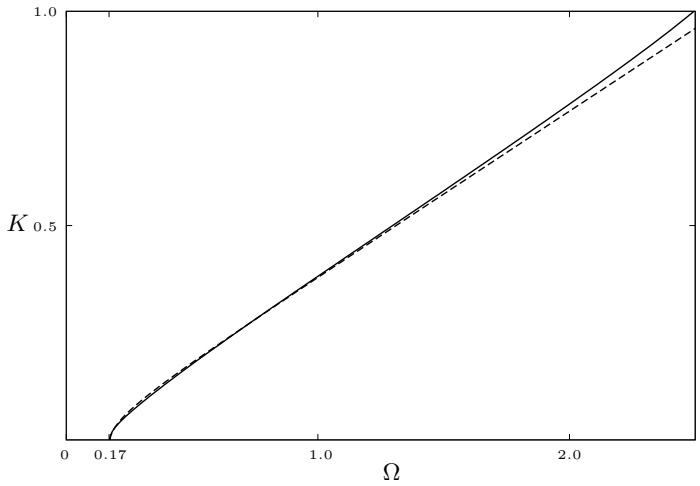

Figure 10: Dispersion curves of the local asymptotic expansion (37) (dashed line) and the Rayleigh-Lamb dispersion relation (17) (solid line)

The obtained results are also useful for estimating the cross thickness variations of plate displacements. As an example, consider the fundamental mode at the lowest cut-off frequency $\Omega = \Omega_{sh}$. As might be expected, the derived two-mode uniform approximation (31) should result in polynomial displacement variations characteristic of long-wave low-frequency behaviour.

First, we have at leading order from (31)

$$\Omega = \varepsilon^{1/2}\left(\frac{r_0}{h}\right)^{1/2}, \qquad K = \varepsilon^{1/4}\left(\frac{3}{(1-\varkappa_s^2)h^3}\right)^{1/4}. \tag{41}$$

On substituting the latter into the formulae (21) and (22), we get

$$u_{1c} = -\varepsilon\,\frac{\chi}{4}, \qquad u_{1s} = \varepsilon\,\frac{2\chi - h - 2}{4h}, \tag{42}$$

and

$$u_{2q} = \varepsilon^{3/4}\,\frac{i}{6}\left(\frac{27(1-\varkappa_s^2)}{h}\right)^{1/4}, \qquad q = c, s \tag{43}$$

for the horizontal and vertical displacements, respectively.

Numerical comparison with the exact solutions (21) and (22) at $\Omega = \Omega_{sh} \approx 0.17$ and $K \approx 0.43$ is given in Figures 11 and 12. The normalised displacements

$$U_1 = \varepsilon^{-1}\begin{cases} u_{1c}, & \text{for } |\chi| \le 1 \\ u_{1s}, & \text{for } 1 \le |\chi| \le 1+h, \end{cases}, \qquad U_2 = \varepsilon^{-3/4}\,|u_{2q}|, \qquad q = c, s \tag{44}$$

are plotted for the same as above set of problem parameters. We don't present here
165 the variation of U_1 at $\Omega = \Omega_{sh}$ which is virtually identical to that in Figure 5.

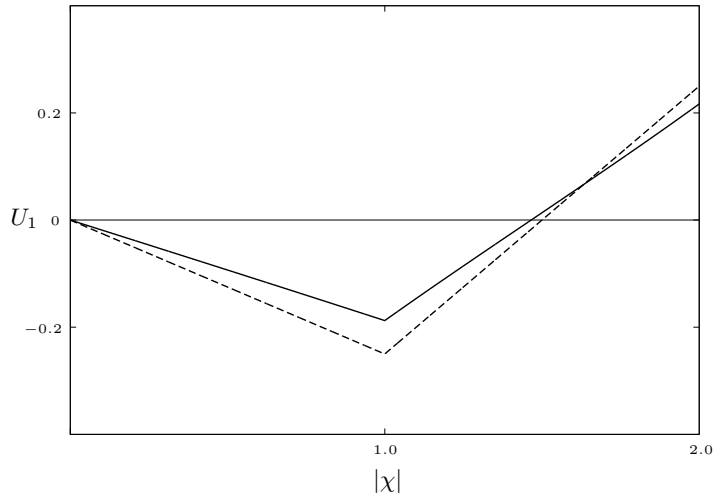

Figure 11: The scaled horizontal displacement (44) calculated by the formulae (42) (dashed line) and (21) (solid line) for the fundamental mode at $\Omega = 0.17$ and $K = 0.43$

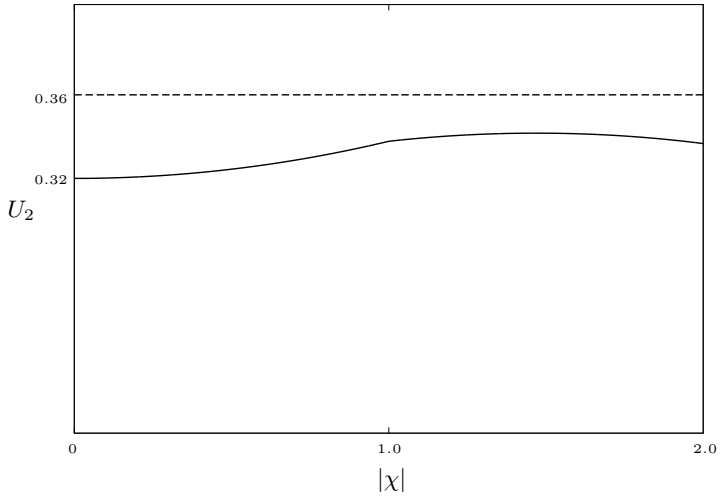

Figure 12: The scaled vertical displacement (44) calculated by the formulae (43) (dashed line) and (22) (solid line) for the fundamental mode at $\Omega = 0.17$ and $K = 0.43$

6. Stiff thin skin layers and light core layer ($\varepsilon \ll 1$, $h \sim \varepsilon$, and $r \sim \varepsilon^2$)

For the chosen set of contrast parameters the local approximations are asymptotically justified only over the narrow non-overlapping vicinities of $\Omega = 0$ and $\Omega = \Omega_{sh} \sim \varepsilon^{1/2}$, see (26). These are given by

$$G_1\Omega^2 + G_2\varepsilon K^4 = 0, \quad \Omega \ll \varepsilon^{1/2}, \tag{45}$$

and

$$G_1\varepsilon + \varepsilon K^2\left(G_3 + \frac{r_0}{h_0}G_8\right) + G_5\Omega^2 = 0, \qquad \Omega - \Omega_{sh} \ll \varepsilon^{1/2}, \tag{46}$$

for the fundamental mode and the first harmonic, respectively, see Table 2. In the above

$$\begin{gathered} G_1 = -\frac{h_0^6}{r_0^3}, \qquad G_2 = -\frac{4}{3}\frac{h_0^5(3h_0\varkappa_s^2 + \varkappa_c^2 - 3h_0 - 1)}{r_0^2}, \\ G_3 = \frac{2h_0^6(2h_0\varkappa_s^2 - 2h_0 - 1)}{r_0^3}, \qquad G_5 = \frac{h_0^7}{r_0^4}, \qquad G_8 = \frac{1}{3}\frac{h_0^7(\varkappa_c^2 + 1)}{r_0^4} \end{gathered} \tag{47}$$

and

$$r_0 = \frac{r}{\varepsilon^2}, \quad h_0 = \frac{h}{\varepsilon}. \tag{48}$$

Order of γ_i	Terms	Fundamental mode $K \sim \varepsilon^{-1/4}\Omega^{1/2}$ $\Omega \ll \varepsilon^{1/2}$	Harmonic $K \sim \left(\Omega^2 - \Omega_{sh}^2\right)^{1/2}\varepsilon^{-1/2}$ $\Omega - \Omega_{sh} \ll \varepsilon^{1/2}$
$\gamma_1 \sim \varepsilon^4$	$\gamma_1\Omega^2$	ε^5K^4	ε^5
$\gamma_2 \sim \varepsilon^5$	γ_2K^4	ε^5K^4	ε^5K^4
$\gamma_3 \sim \varepsilon^4$	$\gamma_3K^2\Omega^2$	ε^5K^6	ε^5K^2
$\gamma_4 \sim \varepsilon^5$	γ_4K^6	ε^5K^6	ε^5K^6
$\gamma_5 \sim \varepsilon^3$	$\gamma_5\Omega^4$	ε^5K^8	ε^5
$\gamma_6 \sim \varepsilon^4$	$\gamma_6K^4\Omega^2$	ε^5K^8	ε^5K^4
$\gamma_7 \sim \varepsilon^5$	γ_7K^8	ε^5K^8	ε^5K^8
$\gamma_8 \sim \varepsilon^3$	$\gamma_8\Omega^4K^2$	ε^5K^{10}	ε^5K^2
$\gamma_9 \sim \varepsilon^4$	$\gamma_9K^6\Omega^2$	ε^5K^{10}	ε^5K^6
$\gamma_{10} \sim \varepsilon^5$	$\gamma_{10}K^{10}$	ε^5K^{10}	ε^5K^{10}

Table 2: Asymptotic behaviour at $\varepsilon \ll 1$, $h \sim \varepsilon$, and $r \sim \varepsilon^2$

Thus, a uniform two-mode asymptotic expansion, similar to that in the previous section, can not be constructed. As an alternative, we proceed with a composite expansion

$$G_1\varepsilon\Omega^2 + G_2\varepsilon^2K^4 + \varepsilon K^2\Omega^2\left(G_3 + \frac{r_0}{h_0}G_8\right) + G_5\Omega^4 = 0 \tag{49}$$

with $\Omega_{sh} \approx \varepsilon^{1/2}\left(\dfrac{r_0}{h_0}\right)^{1/2}$, see Van Dyke (1975), Andrianov et al. (2013) and references therein. This dispersion equation does not approximate the fundamental mode near the first shear cut-off, i.e. at $\Omega \sim \varepsilon^{1/2}$. A typical gap in the validity range of the composite expansion (49), similar to that for a homogeneous plate in

Figure 1, is observed in Figure 13 at $\varepsilon = 0.014$, $h = 0.01$, $r = 0.0002$, $\varkappa_c \approx 0.53$, and $\varkappa_s \approx 0.46$.

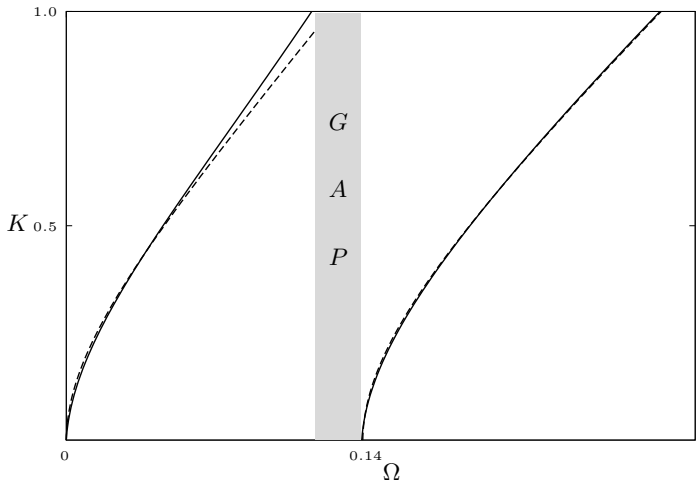

Figure 13: The dispersion curves for the two-mode approximation (49) (dashed line) and the Rayleigh-Lamb dispersion relation (17) (solid line) at $\varepsilon = 0.014$, $h = 0.01$, $r = 0.0002$, $\varkappa_c \approx 0.53$, and $\varkappa_s \approx 0.46$

As in the previous section, it is instructive to evaluate the displacements in the fundamental mode at $\Omega = \Omega_{sh} \approx 0.14$, $K \approx 1.18$. As might be expected for
175 a composite approximation, the cross-sectional variation of the scaled horizontal displacement (44) in Figure 14 calculated by (21) is far from a piecewise linear one. At the same time, computations show that for the first harmonic it is almost identical to the piecewise linear shape in Figure 5.

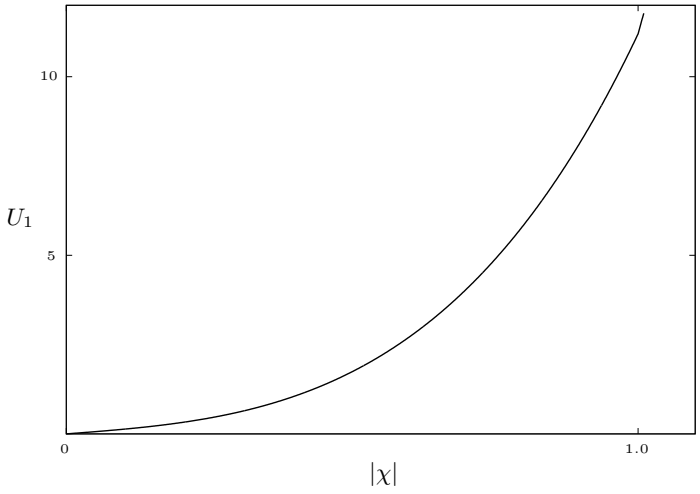

Figure 14: The scaled horizontal displacement (44) calculated by the formulae (21) for the fundamental mode at $\Omega \approx 0.14$ and $K \approx 1.18$

7. Stiff skin layers and thin light core layer ($\varepsilon \ll 1$, $h \sim \varepsilon^{-1/2}$, and $r \sim \varepsilon^{1/2}$)

Order of γ_i	Terms	Fundamental mode $K \sim \varepsilon^{3/8}\Omega^{1/2}$ $\Omega \ll \varepsilon^{1/4}$	Harmonic $K \sim \varepsilon^{1/4}\left(\Omega^2 - \Omega_{sh}^2\right)^{1/2}$ $\Omega \leq \Omega \ll \varepsilon^{3/8}$
$\gamma_1 \sim \varepsilon^6$	$\gamma_1\Omega^2$	$\varepsilon^{9/2}K^4$	$\varepsilon^{11/2}(K^2 + \varepsilon^{3/2})$
$\gamma_2 \sim \varepsilon^{9/2}$	$\gamma_2 K^4$	$\varepsilon^{9/2}K^4$	$\varepsilon^{9/2}K^4$
$\gamma_3 \sim \varepsilon^{9/2}$	$\gamma_3 K^2\Omega^2$	$\varepsilon^3 K^6$	$\varepsilon^4 K^2(K^2 + \varepsilon^{3/2})$
$\gamma_4 \sim \varepsilon^3$	$\gamma_4 K^6$	$\varepsilon^3 K^6$	$\varepsilon^3 K^6$
$\gamma_5 \sim \varepsilon^5$	$\gamma_5\Omega^4$	$\varepsilon^2 K^8$	$\varepsilon^4(K^2 + \varepsilon^{3/2})^2$
$\gamma_6 \sim \varepsilon^{7/2}$	$\gamma_6 K^4\Omega^2$	$\varepsilon^2 K^8$	$\varepsilon^3 K^4(K^2 + \varepsilon^{3/2})$
$\gamma_7 \sim \varepsilon^2$	$\gamma_7 K^8$	$\varepsilon^2 K^8$	$\varepsilon^2 K^8$
$\gamma_8 \sim \varepsilon^4$	$\gamma_8\Omega^4 K^2$	εK^{10}	$\varepsilon^3 K^2(K^2 + \varepsilon^{3/2})^2$
$\gamma_9 \sim \varepsilon^{5/2}$	$\gamma_9 K^6\Omega^2$	εK^{10}	$\varepsilon^2 K^6(K^2 + \varepsilon^{3/2})$
$\gamma_{10} \sim \varepsilon$	$\gamma_{10} K^{10}$	εK^{10}	εK^{10}

Table 3: Asymptotic behaviour at $\varepsilon \ll 1$, $h \sim \varepsilon^{-1/2}$, and $r \sim \varepsilon^{1/2}$

Now, in contrast to the consideration above, we have from (28) $\Omega \ll \varepsilon^{1/4}$ and $K \ll \varepsilon^{1/2}$, instead of usual restrictions $\Omega \ll 1$ and $K \ll 1$.

Inspection of the entries in Table 3 with $\Omega_{sh} \sim \varepsilon^{1/2}$, see (26), leads to the two-mode uniform approximation

$$G_1\varepsilon^3\Omega^2 + G_2\varepsilon^{3/2}K^4 + G_3\varepsilon^{3/2}K^2\Omega^2 + G_4K^6 + G_5\varepsilon^2\Omega^4 = 0, \tag{50}$$

where G_i are now given by

$$\begin{aligned} G_1 &= -\frac{h_0^6}{r_0^3}, \qquad G_2 = -\frac{4}{3}\frac{h_0^8(\varkappa_s^2 - 1)}{r_0^2}, \qquad G_3 = \frac{4h_0^7(\varkappa_s^2 - 1)}{r_0^3}, \\ G_4 &= \frac{4}{3}\frac{h_0^9(\varkappa_s^2 - 1)^2}{r_0^2}, \qquad G_5 = \frac{h_0^7}{r_0^4}, \end{aligned} \tag{51}$$

with $h_0 = \varepsilon^{1/2}h$ and $r_0 = \varepsilon^{-1/2}r$. The dispersion curves originating from the shortened polynomial equation (50) and the Rayleigh-Lamb dispersion relation (17) are plotted in Figure 15 at $\varepsilon = 0.001$, $h = 10.0$, $r = 0.01$, $\varkappa_c \approx 0.60$, and $\varkappa_s \approx 0.60$.

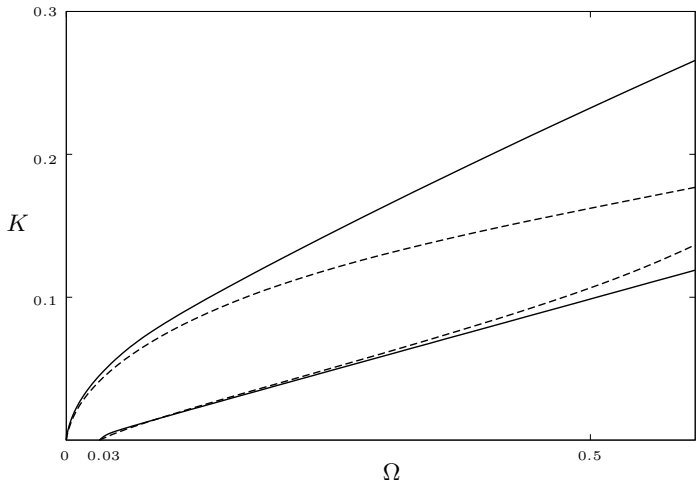

Figure 15: The dispersion curves for the uniform two-mode approximation (50) (dashed line) and the Rayleigh-Lamb dispersion relation (17) (solid line) at $\varepsilon = 0.001$, $h = 10.0$, $r = 0.01$, $\varkappa_c \approx 0.60$, and $\varkappa_s \approx 0.60$

As in Section 6, the uniform approximation (50) involves two local approximations of the fundamental mode:

$$G_1\varepsilon^{3/2}\Omega^2 + G_2K^4 = 0, \quad 0 \le \Omega \ll \varepsilon^{3/4} \tag{52}$$

and

$$G_3\varepsilon^{3/2}\Omega^2 + G_4K^4 = 0, \quad \varepsilon^{3/4} \ll \Omega \ll \varepsilon^{1/4}, \tag{53}$$

as well as the local approximation of the first harmonic

$$\varepsilon^{3/2}G_1 + G_3K^2 + \varepsilon^{1/2}G_5\Omega^2 = 0, \quad \Omega_{sh} \ll \Omega \ll \varepsilon^{3/8}. \tag{54}$$

At $\Omega \sim \varepsilon^{3/8}$ the term with the factor γ_6 in Table 3 should be retained. Also, the first term in the last equation can be neglected at $\Omega \gg \varepsilon^{1/2}$.

8. Soft thin skin layers and light core layer ($\varepsilon \gg 1$, $h \sim \varepsilon^{-2}$, and $r \sim \varepsilon^{-3}$)

Order of γ_i	Terms	Fundamental mode $K \sim \eta^{-1/4}\Omega^{1/2}$ $\Omega \ll \eta^{1/2}$	Harmonic $K \sim \eta^{-1/2}\left(\Omega^2 - \Omega_{sh}^2\right)^{1/2}$ $\Omega - \Omega_{sh} \ll \eta$
$\gamma_1 \sim \eta$	$\gamma_1\Omega^2$	η^2K^4	η^2
$\gamma_2 \sim \eta^2$	γ_2K^4	η^2K^4	η^2K^4
$\gamma_3 \sim \eta$	$\gamma_3K^2\Omega^2$	η^2K^6	η^2K^2
$\gamma_4 \sim \eta^2$	γ_4K^6	η^2K^6	η^2K^6
$\gamma_5 \sim 1$	$\gamma_5\Omega^4$	η^2K^8	η^2
$\gamma_6 \sim \eta$	$\gamma_6K^4\Omega^2$	η^2K^8	η^2K^4
$\gamma_7 \sim \eta^2$	γ_7K^8	η^2K^8	η^2K^8
$\gamma_8 \sim 1$	$\gamma_8\Omega^4K^2$	η^2K^{10}	η^2K^2
$\gamma_9 \sim \eta$	$\gamma_9K^6\Omega^2$	η^2K^{10}	η^2K^6
$\gamma_{10} \sim \eta^2$	$\gamma_{10}K^{10}$	η^2K^{10}	η^2K^{10}

Table 4: Asymptotic behaviour at $\varepsilon \gg 1$, $h \sim \varepsilon^{-2}$, and $r \sim \varepsilon^{-3}$

In this case it is more convenient to operate with the small parameter $\eta = \varepsilon^{-1}$. As in Section 6, we arrive at a composite expansion, see Table 4 with $\Omega_{sh} \sim \eta^{1/2}$. It is

$$G_1\eta\Omega^2 + G_2\eta^2K^4 + K^2\Omega^2\eta\left(G_3 + \frac{r_0}{h_0}G_8\right) + G_5\Omega^4 = 0, \tag{55}$$

where $r_0 = r\varepsilon^3$, $h_0 = h\varepsilon^2$ and

$$G_1 = -\frac{h_0^6}{r_0^3}, \qquad G_2 = -\frac{4}{3}\frac{h_0^5(\varkappa_c^2 - 1)}{r_0^2}, \qquad G_3 = -\frac{2h_0^6}{r_0^3},$$
$$G_5 = \frac{h_0^7}{r_0^4}, \qquad G_8 = \frac{1}{3}\frac{h_0^7(\varkappa_c^2 + 1)}{r_0^4}.$$

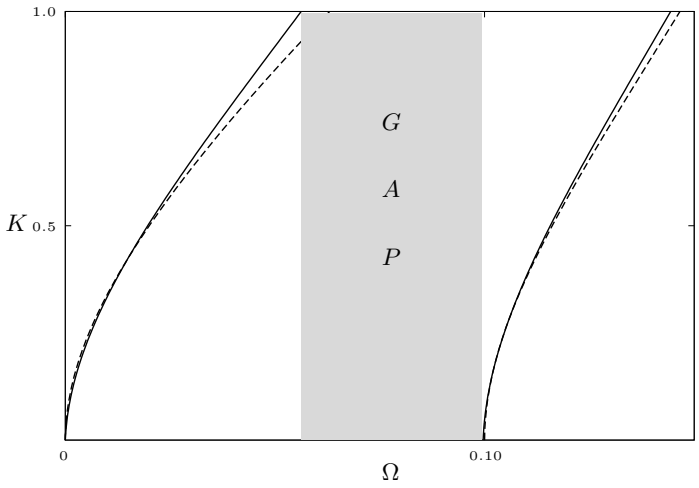

Figure 16: The dispersion curves for the two-mode approximation (55) (dashed line) and the Rayleigh-Lamb dispersion relation (17) (solid line) at $\varepsilon = 100.0$, $h = 0.0001$, $r = 0.000001$, $\varkappa_c \approx 0.60$, and $\varkappa_s \approx 0.60$.

The associated local approximations take the form

$$G_1\Omega^2 + G_2\eta K^4 = 0, \quad 0 \le \Omega \ll \eta^{1/2} \tag{56}$$

and

$$G_1\eta + K^2\eta\left(G_3 + G_8\frac{r_0}{h_0}\right) + G_5\Omega^2 = 0, \quad \Omega - \Omega_{sh} \ll \sqrt{\eta}, \tag{57}$$

where at leading order $\Omega_{sh} = \eta^{1/2}\left(\dfrac{r_0}{h_0}\right)^{1/2}$.

A numerical illustration typical for non-uniform approximations, see also Figure 13, is displayed in Figure 16 for $\varepsilon = 100.0$, $h = 0.0001$, $r = 0.000001$, $\varkappa_c \approx 0.60$, $\varkappa_s \approx 0.60$.

9. Two-mode plate models

The uniformly valid polynomial dispersion relations developed in Sections 5 and 7 along with linear transverse variations of the displacements, see (27), (42) and (43), appear to be a right starting point for deriving related asymptotic plate theories. Here we only sketch 1D equations of motion without making a further insight into all peculiarities of a pretty sophisticated asymptotic methodology, e.g. see Kaplunov et al. (1998) and references therein.

Let us insert into the dispersion relations (31) and (50) the substitutions

$$\Omega^{2n} \to (-1)^n\frac{\partial^{2n}w}{\partial\tau^{2n}}, \qquad K^{2n} \to (-1)^n\frac{\partial^{2n}w}{\partial\xi^{2n}}, \qquad n = 1, 2, 3, ..., \tag{58}$$

where $w(\xi,t)$ is the vertical mid-plane displacement, τ and ξ are dimensionless time and horizontal coordinate. Then, we have from (31) and (50)

$$G_4\frac{\partial^6 w}{\partial\xi^6}-\varepsilon G_2\frac{\partial^4 w}{\partial\xi^4}-G_3\frac{\partial^4 w}{\partial\xi^2\partial\tau^2}-G_5\frac{\partial^4 w}{\partial\tau^4}+\varepsilon G_1\frac{\partial^2 w}{\partial\tau^2}=0 \tag{59}$$

and

$$G_4\frac{\partial^6 w}{\partial\xi^6}-\varepsilon^{3/2} G_2\frac{\partial^4 w}{\partial\xi^4}-\varepsilon^{3/2} G_3\frac{\partial^4 w}{\partial\xi^2\partial\tau^2}-\varepsilon^{2} G_5\frac{\partial^4 w}{\partial\tau^4}+\varepsilon^{3} G_1\frac{\partial^2 w}{\partial\tau^2}=0 \tag{60}$$

respectively.

It is worth considering the static limit of these equations, in which $\dfrac{\partial^{2n} w}{\partial\tau^{2n}}=0$. For example, we obtain from (59)

$$\frac{d^4}{d\xi^4}\left(G_4\frac{d^2 w}{d\xi^2}-\varepsilon G_2 w\right)=0. \tag{61}$$

The last sixth order differential equation may be split into fourth order and second order equations. The first of them

$$\frac{d^4 w}{d\xi^4}=0 \tag{62}$$

corresponds to the classical theory for plate bending, while the second one

$$G_4\frac{d^2 w}{d\xi^2}-\varepsilon G_2 w=0 \tag{63}$$

governs slowly varying evanescent solutions with a typical wave-length, which is $\varepsilon^{-1/2}$ times greater than the plate thickness.

Similarly, the composite plate models originating from the dispersion relations (49) and (55), become

$$\varepsilon^2 G_2\frac{\partial^4 w}{\partial\xi^4}+G_5\frac{\partial^4 w}{\partial\tau^4}+\varepsilon\left(G_3+\frac{r_0}{h_0}G_8\right)\frac{\partial^4 w}{\partial\xi^2\partial\tau^2}-\varepsilon G_1\frac{\partial^2 w}{\partial\tau^2}=0 \tag{64}$$

and

$$\eta^2 G_2\frac{\partial^4 w}{\partial\xi^4}+G_5\frac{\partial^4 w}{\partial\tau^4}+\eta\left(G_3+\frac{r_0}{h_0}G_8\right)\frac{\partial^4 w}{\partial\xi^2\partial\tau^2}-\eta G_1\frac{\partial^2 w}{\partial\tau^2}=0 \tag{65}$$

It is interesting that the static limit of the latter is given by the fourth order equation (62).

10. Concluding remarks

In contrast to a homogeneous plate, the low-frequency vibration spectrum of the considered strongly inhomogeneous three-layered plate involves not only the fundamental bending mode, but also the first harmonic arising at the lowest shear thickness resonance. An asymptotic approach for deriving two-mode polynomial

approximations of the transcendental Rayleigh-Lamb dispersion relation is developed. Four types of high contrast inspired by modern industrial applications, are thoroughly investigated. Two-mode approximations can be both uniform or non-uniform (composite) depending on contrast parameters. The latter are not asymptotically justified for studying the fundamental mode near the lowest shear cut-off. It is remarkable that the leading order uniform approximations analysed in the paper are given by six-order polynomials in wave number, while all the considered composite approximations are forth-order polynomials. A good agreement of asymptotic results and the numerical data obtained from the Rayleigh-Lamb equation is demonstrated.

The 1D partial differential equations corresponding to the shortened polynomial dispersion relations, reveal a clear potential for developing more general two-mode asymptotic models for strongly inhomogeneous layered plates. Such models would be apparently useful for mathematical justification and refinement of various ad hoc shear deformation theories, e.g. see Qatu (2004), Reddy (2004). In this case a key challenge may be concerned with formulation of consistent boundary conditions for six-order equations of motion starting from an appropriate version of the Saint-Venant's principle, e.g. see Gregory & Wan (1985) , Babenkova & Kaplunov (2004) and references therein.

The proposed methodology is not restricted to four high-contrast setups of a three-layered plate considered in the paper. A number of extensions, including asymmetric multi-layered structures, subject to a variety of interfacial conditions, seems to be of interest for advanced technologies. However, one should not always expect a uniform approximation for a high-contrast scenario.

Appendix A Polynomial coefficients

$$\gamma_1 = -\varepsilon h^5 s^4 (hs^2 + \varepsilon),$$

$$\gamma_2 = -\frac{4}{3}\varepsilon h^5 s^4 \Big(h(h^2 + 3h + 3)(\varkappa_s^2 - 1) + \varepsilon(\varkappa_c^2 - 1) \Big),$$

$$\begin{aligned}\gamma_3 = \frac{2}{3} h^5 s^4 \Big(&\varepsilon s^2 h^3 (2\varkappa_s^2 - 3) + 3h^2 \big((\varkappa_s^2 - 1)(\varepsilon^2 + 2s^2) - s^2 \varepsilon \varkappa_s^2 \big) - \\ &3\varepsilon h(-2\varkappa_s^2 + s^2 + 2) + \varepsilon^2 (2\varkappa_c^2 - 3) \Big),\end{aligned}$$

$$\begin{aligned}\gamma_4 = \frac{4}{15} h^5 s^4 \Big(&\varepsilon h (1 - \varkappa_s^2) \big(10h\varkappa_c^2 (1 - \varepsilon) + 5h^3 \varkappa_s^2 + 10h^2 + 10\varepsilon h + 5 + h^4 \big) + \\ &5h^4 \varkappa_s^2 (\varkappa_s^2 - 2) + \varepsilon^2 (1 - \varkappa_c^2) + 5h^4 \Big),\end{aligned}$$

$$\gamma_5 = \frac{1}{6} h^5 s^4 \Big(\varepsilon^2 \big(3s^2 (\varkappa_s^2 + 1) h^2 + \varkappa_c^2 + 3 \big) + \varepsilon h s^2 \big(h^2 s^2 (\varkappa_s^2 + 3) + 3\varkappa_c^2 + 9 \big) + 6h^2 s^4 \Big),$$

$$\begin{aligned}\gamma_6 = \frac{1}{15} s^4 h^5 \Big(&2\varepsilon^2 (\varkappa_c^4 - 4) + \varkappa_c^2 \big(4\varepsilon(\varepsilon - 5h^2 s^2 \varkappa_s^2) + 10\varepsilon^2 h^2 s^2 (\varkappa_s^2 + 1) + \\ &10h(\varkappa_s^2 - 1)(-4\varepsilon^2 h + \varepsilon h^2 + 2hs^2 + 5\varepsilon h + \varepsilon) \big) + \\ &h^3 \varkappa_s^4 (2\varepsilon h^2 s^2 + 25\varepsilon h s^2 + 5\varepsilon^2 h + 10\varepsilon s^2 - 20hs^2) + \\ &2h(\varkappa_s^2 - 1)(2\varepsilon h^4 s^2 + 30h^3 s^2 + 30\varepsilon^2 h + 15\varepsilon h^2 + 10hs^2 - 5\varepsilon h + 15\varepsilon) + \\ &10\varepsilon h^2 s^2 \varkappa_s^2 (2h - 4h^2 - \varepsilon) - 5\varepsilon^2 h^2 (h^2 + 2s^2) + \varepsilon h s^2 (5h^3 - 4h^4 - 50h^2 - 10) + 20h^4 s^2 \Big),\end{aligned}$$

$$\begin{aligned}\gamma_7 = \frac{4}{315} h^5 s^4 \Big(&\varkappa_c^2 \big(35\varepsilon^2 h^4 (\varkappa_s^4 - 1) + 35h^4 (\varkappa_s^4 + 1) + 70h^4 \varkappa_s^2 (-\varepsilon \varkappa_s^2 + \varepsilon - 1) + \\ &42\varepsilon h^2 (\varepsilon - 1)(\varkappa_s^2 - 1) - 2\varepsilon^2 \big) - 35h^4 (\varepsilon^2 \varkappa_s^4 - \varkappa_s^4 - \varepsilon^2 - 1) + 14h^6 (\varkappa_s^4 + 1) + \\ &2\varepsilon h (1 - \varkappa_s^2)(7h^5 \varkappa_s^2 + h^6 + 21h^4 + 21\varepsilon h + 35h^2 + 7) + 2\varepsilon^2 - 28h^6 \varkappa_s^2 - 70h^4 \varkappa_s^2 \Big),\end{aligned}$$

$$\gamma_8 = -\frac{1}{30}h^5s^4\Big(4\varepsilon^2\varkappa_c^4 + \varkappa_c^2\big(10h(\varkappa_s^2-1)(\varepsilon^2h+6hs^2+2\varepsilon) + 20\varepsilon^2h^2s^2(\varkappa_s^2+1) +$$
$$10\varepsilon h^2s^2(2h-5)\varkappa_s^2 - 30h^3s^2\varepsilon - 10h^2s^4 - 15hs^2\varepsilon - 3\varepsilon^2\big) +$$
$$2h^4s^4\varkappa_s^4(2\varepsilon h+5) + h^2s^2\varkappa_s^2(-3\varepsilon h^3s^2 - 20\varepsilon h^2s^2 + 20h^2s^2 + 10\varepsilon) +$$
$$5h(\varkappa_s^2-1)(3\varepsilon^2h^3\varkappa_s^2s^2 + 6\varepsilon^2h + 4hs^2 + 4\varepsilon) + 10\varepsilon h^2s^2(\varkappa_s^2+1)(2h\varkappa_s^2 - 2hs^2 - 3\varepsilon) -$$
$$5\varepsilon h^4s^4(\varkappa_s^4-1) - 9\varepsilon h^5s^4 - 10h^4s^2\varepsilon^2 - 40h^4s^4 - 70h^3s^2\varepsilon - 10h^2s^4 - 25hs^2\varepsilon - 9\varepsilon^2\Big),$$

$$\gamma_9 = \frac{2h^5s^4}{315}\Big(2\varepsilon h^7s^2(2\varkappa_s^4 + 2\varkappa_s^2 - 5) + 7h^6\big(\varepsilon^2(\varkappa_s^4-1) + \varepsilon s^2(2\varkappa_s^6 + 5\varkappa_s^4 - 10\varkappa_s^2 + 1) -$$
$$2s^2(\varkappa_s^2-1)(\varkappa_s^4 + 2\varkappa_s^2 - 5)\big) + 21\varepsilon h^5\big(3s^2\varkappa_s^4 + (\varkappa_c^2 + 2s^2 + 3)\varkappa_s^2 - 7s^2 - \varkappa_c^2 - 3\big) +$$
$$h^4\Big\{35\varepsilon^2\big(\varkappa_s^4(3s^2(1-\varkappa_c^2) - 2\varkappa_c^2 + 3) + 3s^2\varkappa_s^2(\varkappa_c^2-1) + 2s^2(\varkappa_c^2-1) + 2\varkappa_c^2 - 3\big) +$$
$$35\varepsilon\big(\varkappa_s^4(5\varkappa_c^2s^2 + 5\varkappa_c^2 - 1) + \varkappa_s^2(-8\varkappa_c^2s^2 - 5\varkappa_c^2 + 1) + s^2\varkappa_c^2\big) -$$
$$35(\varkappa_s^2-1)\big(\varkappa_s^2(2s^2(\varkappa_c^2+1) + 3\varkappa_c^2 + 1) - 4s^2(\varkappa_c^2+1) - 3\varkappa_c^2 - 1\big)\Big\} +$$
$$35\varepsilon h^3\big(\varkappa_s^2(3\varkappa_c^2 + 2s^2 + 5) + s^2\varkappa_s^4 - 5s^2 - 3\varkappa_c^2 - 5\big) +$$
$$h^2\Big\{21\Big(\varepsilon^2\big\{\varkappa_s^2\big(s^2(\varkappa_c^2-1) + 8 - 2\varkappa_c^4 - 4\varkappa_c^2\big) + s^2(\varkappa_c^2-1) - 8 + 2\varkappa_c^4 + 4\varkappa_c^2\big\} +$$
$$\varepsilon\big(\varkappa_s^2(2\varkappa_c^4 - 2\varkappa_c^2s^2 + 7\varkappa_c^2 - 1) + 1 - 2\varkappa_c^4 - 7\varkappa_c^2\big) + 2s^2(\varkappa_s^2-1)(\varkappa_c^2+1)\Big)\Big\} -$$
$$14\varepsilon h(-2\varkappa_s^2\big(\varkappa_c^2+2) + s^2 + 2\varkappa_c^2 + 4\big) + 2\varepsilon^2(2\varkappa_c^4 + 2\varkappa_c^2 - 5)\Big),$$

$$\gamma_{10} = -\frac{4}{2835}h^5s^4\Big(\varepsilon h^9(\varkappa_s^2-1) + 9h^8\big(\varepsilon\varkappa_s^2(\varkappa_s^2-1) - (\varkappa_s^2-1)^2\big) + 36\varepsilon h^7(\varkappa_s^2-1) -$$
$$42h^6(\varkappa_s^2-1)\big((\varkappa_c^2-1)(\varkappa_s^2+1)\varepsilon^2 - 2\varepsilon\varkappa_c^2\varkappa_s^2 + (\varkappa_c^2+1)(\varkappa_s^2-1)\big) +$$
$$126\varepsilon h^5(\varkappa_s^2-1) - 63h^4(\varkappa_s^2-1)\big((\varkappa_c^2-1)(\varkappa_s^2+1)\varepsilon^2 - 2\varepsilon\varkappa_c^2\varkappa_s^2 + (\varkappa_c^2+1)(\varkappa_s^2-1)\big) +$$
$$84\varepsilon h^3(\varkappa_s^2-1) - 36\varepsilon h^2(\varkappa_s^2-1)\big(\varepsilon(\varkappa_c^2-1) - \varkappa_c^2\big) + 9\varepsilon h(\varkappa_s^2-1) + \varepsilon^2(\varkappa_c^2-1)\Big),$$

where $s^2 = \varepsilon/r$.

Appendix B Coefficients in formulae (21) and (22)

$$A_c = a_{1c}D + a_{2c}, \quad B_c = b_{1c}D + b_{2c}, \quad A_s = a_{1s}D + a_{2s}, \quad B_s = b_{1s}D + b_{2s},$$

where

$$a_{1c} = -\frac{ir_4K(S_{\kappa_s}S_{\beta_c}r_6\beta_c h + C_{\kappa_s}C_{\beta_c}r_3\beta_s)}{h(-C_{\alpha_c}S_{\beta_c}r_2r_6\alpha_c\beta_c + C_{\beta_c}S_{\alpha_c}r_3r_5K^2)}, \quad a_{2c} = -\frac{ir_4K(C_{\kappa_s}S_{\beta_c}r_6\beta_c h + C_{\beta_c}S_{\kappa_s}r_3\beta_s)}{h(-C_{\alpha_c}S_{\beta_c}r_2r_6\alpha_c\beta_c + C_{\beta_c}S_{\alpha_c}r_3r_5K^2)},$$

$$b_{1c} = \frac{r_4(K^2S_{\kappa_s}S_{\alpha_c}r_5h + C_{\kappa_s}C_{\alpha_c}r_2\alpha_c\beta_s)}{(C_{\alpha_c}S_{\beta_c}r_2r_6\alpha_c\beta_c - C_{\beta_c}S_{\alpha_c}r_3r_5K^2)h}, \quad b_{2c} = \frac{r_4(C_{\kappa_s}S_{\alpha_c}K^2r_5h + C_{\alpha_c}S_{\kappa_s}r_2\alpha_c\beta_s)}{(C_{\alpha_c}S_{\beta_c}r_2r_6\alpha_c\beta_c - C_{\beta_c}S_{\alpha_c}K^2r_3r_5)h},$$

$$a_{1s} = \frac{i}{2}\frac{4(Q_1^2-1)Q_2\beta_s\alpha_s - K^2h^2r_1^2Q_1Q_3Q_4}{Kh\alpha_sr_1Q_3}, \quad a_{2s} = \frac{i}{2}\frac{4Q_4(Q_1^2-1)\beta_s\alpha_s - K^2h^2r_1^2Q_1Q_2Q_3}{Kh\alpha_sr_1Q_3},$$

$$b_{1s} = -\frac{i}{2}\frac{-K^2Q_3Q_4r_1^2h^2 + 4Q_1Q_2\alpha_s\beta_s}{Kh\alpha_sr_1}, \quad b_{2s} = -\frac{i}{2}\frac{-K^2Q_2Q_3r_1^2h^2 + 4Q_1Q_4\alpha_s\beta_s}{Kh\alpha_sr_1},$$

and

$$D = -\frac{ia_{2c}r_3S_{\alpha_c} + b_{2c}q2r_2S_{\beta_c} + ia_{2s}r_4S_{\theta_s} + ib_{2s}r_4C_{\theta_s}}{ia_{1c}r_3S_{\alpha_c} + b_{1c}q2r_2S_{\beta_c} + ia_{1s}r_4S_{\theta_s} + ib_{1s}r_4C_{\theta_s}}.$$

In the above

$$Q_1 = C_{\theta_s}C_{\alpha_s} + S_{\theta_s}S_{\alpha_s}, \qquad Q_2 = C_{\kappa_s}C_{\beta_s} + S_{\kappa_s}S_{\beta_s},$$

$$Q_3 = S_{\theta_s}C_{\alpha_s} + C_{\theta_s}S_{\alpha_s}, \qquad Q_4 = S_{\kappa_s}C_{\beta_s} + C_{\kappa_s}S_{\beta_s},$$

and

$$r_1 = \frac{\beta_s^2}{K^2h^2} + 1, \quad r_2 = 2(\varepsilon - 1), \quad r_3 = -\frac{\varepsilon(K^2 + \beta_c^2)}{K^2} + 2,$$

$$r_4 = r_1 - 2, \quad r_5 = -r_1 - r_3 + 2, \quad r_6 = r_1 - 2\varepsilon.$$

with $S_{\theta_s} = \sinh(\theta_s)$, $C_{\theta_s} = \cosh(\theta_s)$, $S_{\kappa_s} = \sinh(\kappa_s)$, $C_{\kappa_s} = \cosh(\kappa_s)$.

References

Altenbach, H., Eremeyev, V. A., & Naumenko, K. (2015). On the use of the first order shear deformation plate theory for the analysis of three-layer plates with thin soft core layer. *ZAMM-Journal of Applied Mathematics and Mechanics/Zeitschrift für Angewandte Mathematik und Mechanik*, *95*, 1004–1011.

Andrianov, I. V., Awrejcewicz, J., & Manevitch, L. I. (2013). *Asymptotical mechanics of thin-walled structures*. Springer Science and Business Media.

Aşık, M. Z., & Tezcan, S. (2005). A mathematical model for the behavior of laminated glass beams. *Computers and Structures*, *83*, 1742–1753.

Aßmus, M., Naumenko, K., & Altenbach, H. (2016). A multiscale projection approach for the coupled global–local structural analysis of photovoltaic modules. *Composite Structures*, *158*, 340–358. doi:10.1016/j.compstruct.2016.09.036.

Aßmus, M., Nordmann, J., Naumenko, K., & Altenbach, H. (2017). A homogeneous substitute material for the core layer of photovoltaic

composite structures. *Composites Part B: Engineering*, *112*, 353–372. doi:10.1016/j.compositesb.2016.12.042.

Babenkova, E., & Kaplunov, J. (2004). Low-frequency decay conditions for a semi-infinite elastic strip. *Proceedings of the Royal Society of London A: Mathematical, Physical and Engineering Sciences*, *460*, 2153–2169.

Berdichevsky, V. (2009). *Variational principles of continuum mechanics: I. Fundamentals*. Springer Science & Business Media.

Berdichevsky, V. L. (2010). An asymptotic theory of sandwich plates. *International Journal of Engineering Science*, *48*, 383–404.

Carrera, E., & Brischetto, S. (2009). A survey with numerical assessment of classical and refined theories for the analysis of sandwich plates. *Applied Mechanics Reviews*, *62*, 010803.

Chapman, C. J. (2013). An asymptotic decoupling method for waves in layered media. *Proceedings of the Royal Society of London A: Mathematical, Physical and Engineering Sciences*, *469*, 20120659.

Cherdantsev, M., & Cherednichenko, K. D. (2012). Two-scale Γ-convergence of integral functionals and its application to homogenisation of nonlinear high-contrast periodic composites. *Archive for Rational Mechanics and Analysis*, *204*, 445–478.

Craster, R. V., Joseph, L. M., & Kaplunov, J. (2014). Long-wave asymptotic theories: the connection between functionally graded waveguides and periodic media. *Wave Motion*, *51*, 581–588.

Elishakoff, I., Kaplunov, J., & Nolde, E. (2015). Celebrating the centenary of Timoshenko's study of effects of shear deformation and rotary inertia. *Applied Mechanics Reviews*, *67*, 060802.

Figotin, A., & Kuchment, P. (1998). Spectral properties of classical waves in high-contrast periodic media. *SIAM Journal on Applied Mathematics*, *58*, 683–702.

Graff, K. F. (2012). *Wave motion in elastic solids*. Courier Corporation.

Gregory, R. D., & Wan, F. Y. M. (1985). On plate theories and Saint-Venant's principle. *International Journal of Solids and Structures*, *21*, 1005–1024.

Hohe, J., & Librescu, L. (2004). Advances in the structural modeling of elastic sandwich panels. *Mechanics of Advanced Materials and Structures*, *11*, 395–424.

Kaplunov, J., & Nobili, A. (2016). Multi-parametric analysis of strongly inhomogeneous periodic waveguides with internal cut-off frequencies. *Mathematical Methods in the Applied Sciences*, . doi:10.1002/mma.3900.

Kaplunov, J., Prikazchikov, D., & Sergushova, O. (2016). Multi-parametric analysis of the lowest natural frequencies of strongly inhomogeneous elastic rods. *Journal of Sound and Vibration*, *366*, 264–276.

Kaplunov, J. D., Kossovich, L. Y., & Nolde, E. V. (1998). *Dynamics of thin walled elastic bodies*. Academic Press.

Kreja, I. (2011). A literature review on computational models for laminated composite and sandwich panels. *Open Engineering*, *1*, 59–80.

Kudaibergenov, A., Nobili, A., & Prikazchikova, L. (2016). On low-frequency vibrations of a composite string with contrast properties for energy scavenging fabric devices. *Journal of Mechanics of Materials and Structures*, *11*, 231–243.

Le, K. C. (1999). *Vibrations of shells and rods*. Springer Berlin.

Lee, P., & Chang, N. (1979). Harmonic waves in elastic sandwich plates. *Journal of Elasticity*, *9*, 51–69.

Martin, T. P., Layman, C. N., Moore, K. M., & Orris, G. J. (2012). Elastic shells with high-contrast material properties as acoustic metamaterial components. *Physical Review B*, *85*, 161103.

Milton, G. W. (2002). *The theory of composites*. Cambridge University Press.

Naumenko, K., & Eremeyev, V. A. (2014). A layer-wise theory for laminated glass and photovoltaic panels. *Composite Structures*, *112*, 283–291.

Qatu, M. S. (2004). *Vibration of laminated shells and plates*. Elsevier.

Reddy, J. N. (2004). *Mechanics of laminated composite plates and shells: theory and analysis*. CRC Press.

Ryazantseva, M. Y., & Antonov, F. K. (2012). Harmonic running waves in sandwich plates. *International Journal of Engineering Science*, *59*, 184–192.

Schulze, S. H., Pander, M., Naumenko, K., & Altenbach, H. (2012). Analysis of laminated glass beams for photovoltaic applications. *International Journal of Solids and Structures*, *49*, 2027–2036.

Smyshlyaev, V. P. (2009). Propagation and localization of elastic waves in highly anisotropic periodic composites via two-scale homogenization. *Mechanics of Materials*, *41*, 434–447.

Tovstik, P. E., & Tovstik, T. P. (2016). Generalized Timoshenko-Reissner models for beams and plates, strongly heterogeneous in the thickness direction. *ZAMM-Journal of Applied Mathematics and Mechanics/Zeitschrift für Angewandte Mathematik und Mechanik*, . doi:10.1002/zamm.201600052.

Van Dyke, M. (1975). *Perturbation methods in fluid mechanics*. Parabolic Press, Stanford, CA.

Vinson, J. R. (1999). *The behavior of sandwich structures of isotropic and composite materials*. CRC Press.

Wang, C. M., Reddy, J. N., & Lee, K. H. (2000). *Shear deformable beams and plates: Relationships with classical solutions*. Elsevier.